Spring 2011

Absorbing state transitions in clean and disordered lattice models

Man Young Lee

Department: Physics

Recommended Citation

Lee, Man Young, "Absorbing state transitions in clean and disordered lattice models" (2011). *Doctoral Dissertations*. 2095.
https://scholarsmine.mst.edu/doctoral_dissertations/2095

only via a rare collective fluctuation involving *all* sites of the cluster. We thus expect the long-time decay of the density to be of exponential form (suppressing subleading pre-exponential factors),

$$\rho_s(t) \sim \exp[-t/t_s(s)] \ , \tag{116}$$

with a long lifetime t_s that increases exponentially with the cluster size s

$$t_s(s) = t_0 \exp[A(\lambda)s] \tag{117}$$

for sufficiently large s. Here, t_0 is some microscopic time scale.

The lifetime increases the faster with s the further the cluster is in the active phase. This means, the prefactor $A(\lambda)$ which plays the role of an inverse correlation volume vanishes at the multicritical value λ_* and monotonically increases with increasing λ. Close to the multicritical point, the behavior of $A(\lambda)$ can be inferred from scaling. Since $A(\lambda)$ has the dimension of an inverse volume, it varies as

$$A(\lambda) \sim (\lambda - \lambda_*)^{\nu_* D_f} \tag{118}$$

where ν_* is the correlation length exponent of the multicritical point and D_f is the (fractal) space dimensionality of the underlying cluster.

Note that (117) establishes an exponential relation between length and time scales at the transition. Because the number of sites s of a percolation cluster is related to its linear size R_s via $s \sim R_s^{D_f}$, eq. (117) implies

$$\ln t_s \sim R_s^{D_f} \ . \tag{119}$$

Thus, the dynamical scaling is activated rather than power-law with the tunneling exponent being identical to the fractal dimension of the critical percolation cluster, $\psi = D_f$.

To confirm the above phenomenological arguments, we have performed extensive Monte-Carlo simulations of the contact process on finite-size clusters using clean one-dimensional and two-dimensional systems as well as diluted lattices. Our simulation method is based on the algorithm by Dickman [35] and described in detail in Refs. [28, 29].

A characteristic set of results is shown in Fig. 3.3. It shows the time evolution of the contact process on several one-dimensional clusters of different size s, starting

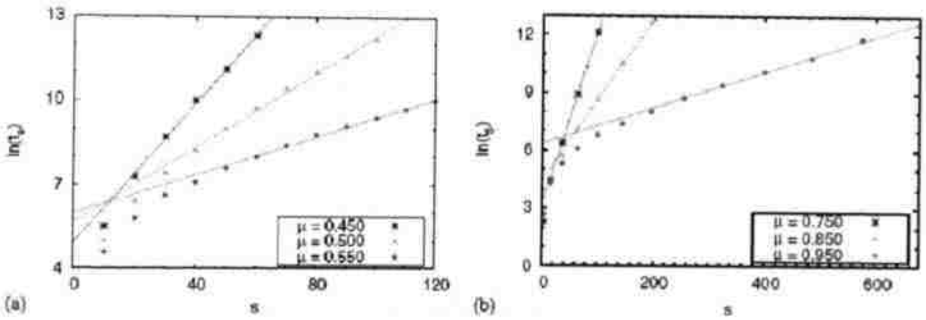

Figure 3.7. (Color online:) Lifetime t_s as a function of cluster size s for the generalized contact process with two inactive states at different values of the healing rate μ. The infection and boundary activation rates are fixed, $\lambda = \sigma = 1$, and the data are averages over 10^6 runs. (a) $d = 1$ where the bulk system has a transition, see Fig. 3.6. (b) $d = 2$, where we do not find a bulk transition because the system is always active [32]. The dashed lines are fits of the large-s behaviors to the exponential law (117).

critical exponents of the nonequilibrium phase transition can be expressed in terms of the classical lattice percolation exponents. Their values are known exactly in two space dimensions and with good numerical accuracy in three space dimensions; they are summarized in Table 3.1.

Thus, our transition in $d = 2$ provides one of the few examples of a nonequilibrium phase transition with exactly known critical exponents.

The logarithmically slow dynamics (125), (136) at criticality together with the small value of the exponent $\bar{\delta}$ make a numerical verification of our theory by simulations of the full diluted lattice a very costly proposition. The results of recent

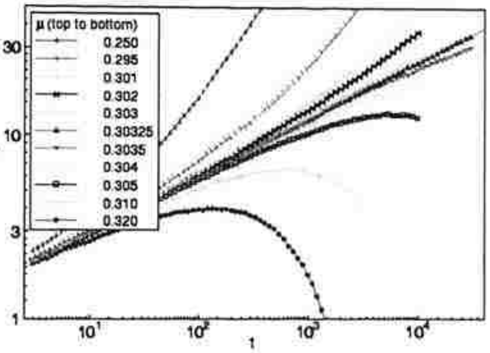

Figure 4.2. (Color online) Spreading simulations at $\sigma = 0$: Number N_s of active sites as a function of time t. The solid line for $\mu = 0.30325$ represents a fit to $N_s \sim t^{\Theta_{cp}}$ yielding $\Theta_{cp} = 0.315(5)$. The data are averages over 25000 runs.

Initially, $N_s(t)$ follows the behavior of the simple contact process at this μ. At later times, the curves with $\sigma \gtrapprox 0.25$ curve upwards implying that the system is in the active phase. The curves for $\sigma \lessapprox 0.25$ curve downward, indicating that the system is in the inactive phase. Thus, $\sigma_c(\mu = 0.6) \approx 0.25$.

In contrast, the set of curves for $\mu = 0.428$ (Fig. 4.3a) behaves very differently. After an initial decay, $N_s(t)$ curves strongly upwards for all values of σ down to the smallest value studied, $\sigma = 10^{-4}$. This suggests that at $\mu = 0.428$, any nonzero σ takes the generalized contact process to the active phase. The phase transition thus occurs at $\sigma = 0$.

We determined analogous sets of curves for many different values of the healing rate in the interval $\mu_c^{cp} = 0.30325 < \mu < 0.65$. We found that the phase transition to the active phase occurs at $\sigma = 0$ for $\mu_c^{cp} < \mu < \mu^* = 0.552$, while it occurs at a nonzero σ for healing rates $\mu > \mu^*$. This establishes the phase diagram shown in Fig. 4.1. The phase boundary thus does *not* follow the simple crossover scenario outlined above. In the following subsections, we analyze in detail the critical behavior of the different nonequilibrium phase transitions.

4.4.3. Generic Transition.

We first consider the generic transition occurring at $\mu > \mu^* \approx 0.552$ and nonzero σ (the blue dashed line in Fig. 4.1). Figure 4.4 shows a set of spreading simulations at $\sigma = 0.1$ and several μ in the vicinity of the phase boundary. The data indicate a critical point at $\mu \approx 0.582$. We performed

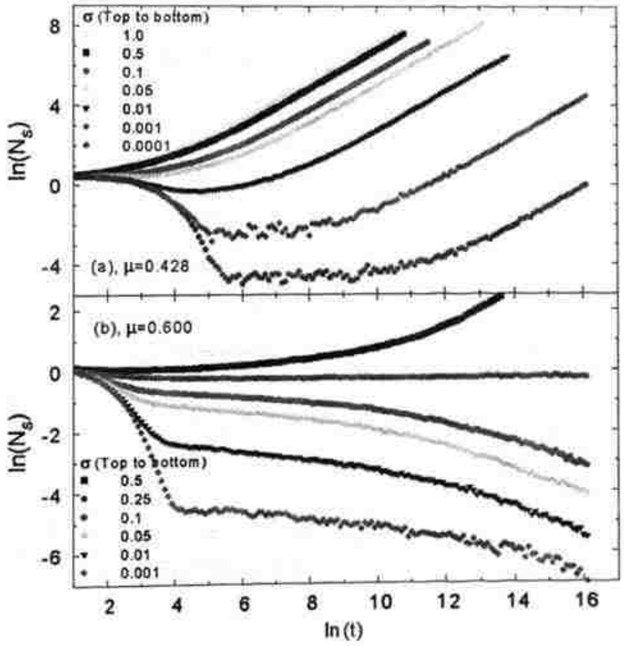

Figure 4.3. (Color online) Spreading simulations: Number N_s of active sites as a function of time t for several σ at fixed $\mu = 0.428$ (panel a) and $\mu = 0.6$ (panel b). The data are averages over 10^3 (at the smallest σ) to 10^5 runs.

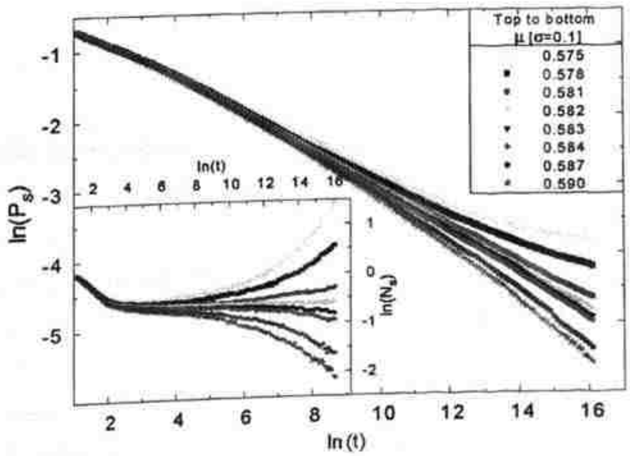

Figure 4.4. (Color online) Spreading simulations at $\sigma = 0.1$ for several μ close to the phase boundary. Main panel: Survival probability P_s as a function of time t. The data are averages over 10^5 runs. Inset: Number N_s of active sites as a function of time t.

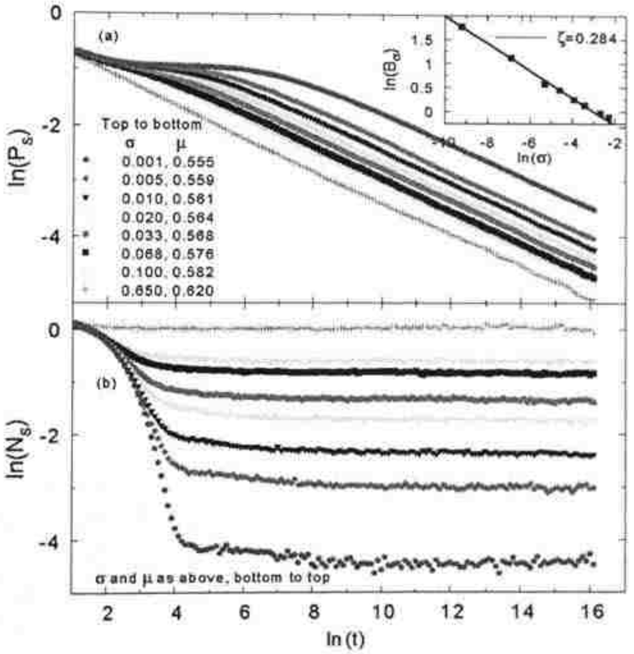

Figure 4.5. (Color online) Critical spreading simulations: Survival probability P_s and number of active sites N_s as functions of t for several points (μ, σ) located on the generic phase boundary. The inset shows the prefactor B_σ of the critical power law $P_s = B_\sigma t^{-\delta}$ as a function of σ. The solid line is a fit to $B_\sigma \sim \sigma^{-\zeta}$ which gives $\zeta = 0.284$.

analogous simulations for several points on the phase boundary. Figure 4.5 shows the survival probability P_s and number N_s of active sites as functions of time for all the respective critical points. In log-log representation, the N_s and P_s curves for different σ and μ are perfectly parallel, i.e., they represent power-laws with the same exponent. Fits of the asymptotic long-time behavior to $P_s = B_\sigma t^{-\delta}$ and $N_s = C_\sigma t^{\Theta}$ give estimates of $\delta = 0.289(5)$ and $\Theta = 0.000(5)$. Moreover, we measured (not shown) the mean-square radius $R^2(t)$ of the active cloud as a function of time. Its long time behavior follows a universal power law. Fitting to $R^2(t) \sim t^{2/z}$ gives $2/z = 1.145(5)$ ($z = 1.747(7)$). Here $z = \nu^{\|}/\nu^{\perp}$ is the dynamical exponent, i.e., the ratio between the correlation time exponent $\nu_{\|}$ and the correlation length exponent $\nu_{\perp}$.

In addition to the spreading simulations, we also performed density decay simulations for several (μ, σ) points on the phase boundary. Characteristic results are

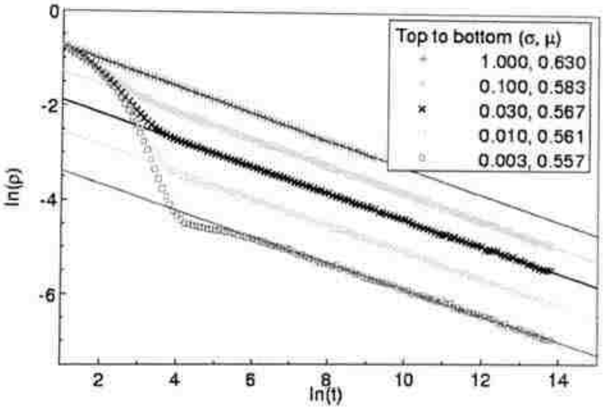

Figure 4.6. (Color online) Critical density decay simulations: Density ρ_A of active sites as function of t for several points (μ, σ) on the generic phase boundary. The solid lines are fits to a power law $\rho_A = \bar{B}_\sigma t^{-\alpha}$ giving $\alpha = 0.285(5)$. The data represent averages of 400 runs with system size $L = 10^4$.

presented in Fig. 4.6. The figure shows that the density ρ_A of active sites at criticality follows a universal power law, $\rho_A = \bar{B}_\sigma t^{-\alpha}$ at long times. The corresponding fits give $\alpha = 0.285(5)$ which agrees (within the error bars) with our value of the survival probability exponent δ. We thus conclude that the generic transition of our system is characterized by three independent exponents (for instance $\nu_\perp, z$ and δ) rather than four (as could be expected for a general absorbing state transition [4]). We point out, however, that even though P_s and ρ_A show the same power-law time dependence at criticality, the behavior of the prefactors differs. Specifically, the prefactor $\bar{B}_\sigma$ of the density is increasing with increasing σ while the prefactor B_σ of the survival probability decreases with increasing σ.

All the exponents of the generic transition do not depend on μ or σ, implying that the critical behavior is universal. Moreover, their values are in excellent agreement with the known values of the PC (or DP2) universality class (see, e.g., Ref. [4, 5]). We therefore conclude that the critical behavior of the generic transition of generalized contact process with two inactive states is universally in this class.

4.4.4. Transition at $\sigma = 0$. After discussing the generic transition, we now turn to the line of transitions at $\mu_c^{cp} < \mu < \mu^*$ and $\sigma = 0$. To investigate these

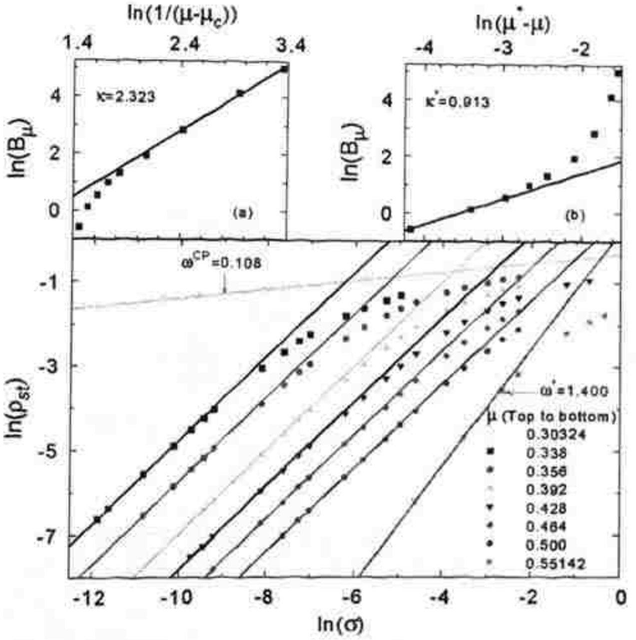

Figure 4.7. (Color online) Density decay simulations. Main panel: stationary density ρ_{st} as a function of the boundary rate σ for various healing rates μ. For $\mu_c^{cp} < \mu < \mu^*$, the solid lines are fits of the low-σ behavior to $\rho_{st} = B_\mu \sigma$. At the simple contact process critical point, $\mu = \mu_c^{cp} = 0.30324$, and at the endpoint, $\mu = \mu^* = 0.552$, we fit to power-laws $\rho_{st} \sim \sigma^\omega$ which gives exponents of $\omega_{cp} = 0.108(2)$ and $\omega^* = 1.4(1)$. The data are averages over 50 to 200 runs with system sizes $L = 2000$ to 5000. Inset a: prefactor B_μ of the linear σ dependence as a function of $\mu - \mu_c^{cp}$. A fit to a power law gives $B_\mu \sim (\mu - \mu_c^{cp})^{-\kappa}$ with $\kappa = 2.32(10)$. Inset b: prefactor B_μ as a function of $\mu^* - \mu$. A fit to a power law gives $B_\mu \sim (\mu^* - \mu)^{\kappa^*}$ with $\kappa^* = 0.91$.

transitions more closely, we performed both spreading and density decay simulations at fixed μ and several σ-values approaching $\sigma = 0$ (as indicated by the solid (red) arrows in the phase diagram, Fig. 4.1).

Let us start by discussing the density decay simulations. Figure 4.7 shows the stationary density ρ_{st} of active sites as a function of σ for several values of the healing rate μ. Interestingly, the stationary density depends linearly on σ for all healing rates $\mu_c^{cp} < \mu < \mu^*$, in seeming agreement with mean-field theory. This means $\rho_{st} = B_\mu \sigma^\omega$ with $\omega = 1$ and B_μ being a μ-dependent constant. We also analyzed, how the prefactor B_μ of the mean-field-like behavior depends on the distance from the simple contact

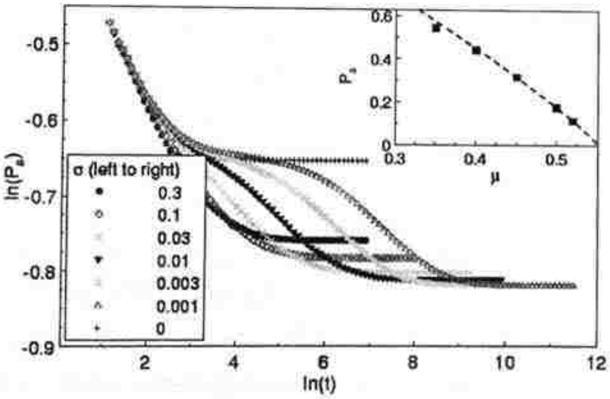

Figure 4.8. (Color online) Spreading simulations: Survival probability P_s as a function of time t at $\mu = 0.4$ for various values of the boundary rate σ. The data are averages over 100000 runs. Inset: Low-σ limit of the stationary P_s as a function of μ. The dashed line is a fit to $P_s \sim (\mu^* - \mu)^\beta$ with $\mu^* = 0.552$ and $\beta = 0.87(5)$ in agreement with the PC universality class (see, e.g., Refs. [4, 5]).

process critical point. As inset a) of Fig. 4.7 shows, B_μ diverges as $(\mu - \mu_c^{cp})^{-\kappa}$ with $\kappa = 2.3(1)$.

At the critical healing rate μ_c^{cp} of the simple contact process, the stationary density displays a weaker σ-dependence. A fit to a power-law $\rho_{st} \sim \sigma^{\omega_{cp}}$ gives an exponent value of $\omega_{cp} = 0.108(2)$. In contrast, at the endpoint at healing rate μ^*, the corresponding exponent $\omega^* = 1.4(1)$ is larger than 1.

These results of the density decay simulations must be contrasted with those of the spreading simulations. Figure 4.8 shows the time dependence of the survival probability P_s for $\mu = 0.4$ and several σ. At early times, all curves follow the $\sigma = 0$ data due to the small values of the rate of the boundary activation process (143). (Note that the $\sigma = 0$ curve does *not* reproduce the survival probability of the simple contact process. This is because in our generalized contact process, a sample is surviving as long as not every site is in state I_1 even if there are no active sites.) In the long-time limit, the P_s curves approach nonzero constants, as expected in an active phase. However, in contrast to the stationary density ρ_{st} (Fig. 4.7), the stationary value of P_s does not go to zero with vanishing boundary σ. Instead, it approaches a

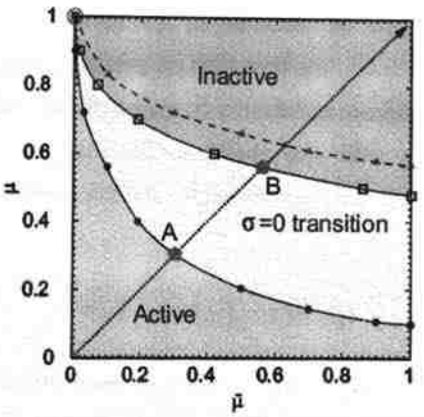

Figure 4.9. (Color online) Projection of the phase diagram of the generalized contact process on the $\bar{\mu} - \mu$ plane. The individual symbols show the locations of the phase boundaries as determined from our simulations: solid blue circles – transition for $\sigma \equiv 0$ (simple contact process), solid red triangles – generic transition for $\sigma = 1$, open squares – approximate location of the endpoint of the generic transition ($\sigma \to 0$) estimated from the transition at $\sigma = 0.01$. The lines are guides to the eye only. Points A and B are the simple contact process critical point and the endpoint investigated in the main part of the paper.

to the usual contact process in the limit of $\sigma \to 0$. In order to study how general our results are, we have performed a few simulation runs for $\bar{\mu} \neq \mu$ focusing on the fate of the endpoint that separates the generic transition from the $\sigma = 0$ transition. The results of these runs are summarized in Fig. 4.9 which shows the phase diagram projected on the $\bar{\mu} - \mu$ plane.

The figure shows that the line of endpoints of the generic phase boundary remains distinct from the simple contact process ($\sigma = 0$) critical line in the entire $\bar{\mu} - \mu$ plane. The two lines only merge at the point $\bar{\mu} = 0, \mu = 1$ where the system behaves as compact directed percolation [13].

Our study was started because simulations at $\mu \gtrapprox \mu_c^{cp}$ and $\sigma \ll 1$ [18] seemed to suggest that the generalized contact process with two absorbing states is always active for any nonzero σ. The detailed work reported in this paper shows that this is *not* the case; a true inactive phase appears, but only at significantly higher $\mu > \mu^*$. Motivated by this result, we also carefully reinvestigated the generalized contact process with $n = 3$ absorbing states which has been reported to be always active (for any nonzero

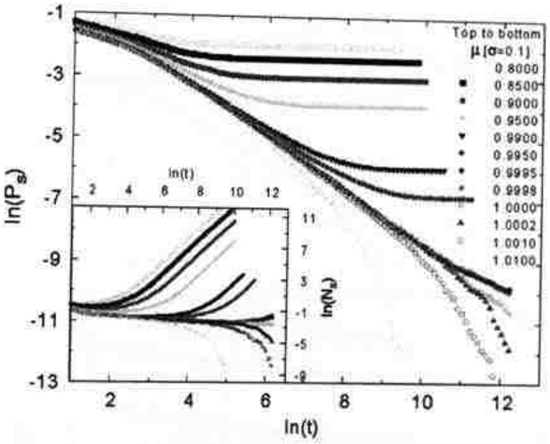

Figure 5.2. (Color online) Spreading simulations at $\sigma = 0.1$ for several μ close to the phase boundary. Main panel: Number N_s of active sites as a function of time t. Inset: Survival probability P_s as a function of time t. The data close to criticality are averages over 10^6 runs on a 4000×4000 system, smaller numbers of runs were used away from criticality.

To test this prediction we compare in Fig. 5.4 plots of $\ln(P_s\, t)$ vs. $\ln(t)$ (straight lines corresponds to power laws) and $P_s\, t$ vs. $\ln(t)$ (straight lines correspond to logarithmic behavior). Although both functional forms describe the long-time data reasonably well, the curves in the $\ln(P_s\, t)$ vs. $\ln(t)$ plot show a systematic downward curvature. Moreover, the semi-logarithmic plot, $P_s\, t$ vs. $\ln(t)$, leads to straight lines over a longer time interval which we take as evidence for GV critical behavior. We performed an analogous analysis for number of active sites N_s. Again, both a simple power law and mean-field behavior with logarithmic corrections describe the data reasonably well, with the quality of fits being somewhat higher for the latter case. We also measured (not shown) the mean-square radius $R^2(t)$ of the active cloud as a function of time. A pure power-law fit of its long time behavior, $R^2(t) \sim t^{2/z}$, gives $2/z = 0.97(4)$ ($z = 2.06(8)$). The data can be described equally well by mean-field behavior $R^2(t) \;\sim t$ with logarithmic corrections.

In addition to the spreading runs, we also performed density decay runs at the generic phase boundary. The resulting density of active sites ρ as a function of time can be fitted with a pure power law $\rho(t) \sim t^{-\alpha}$ giving a very small value of $\alpha = 0.080(4)$. A better fit is achieved with the simple logarithmic time dependence

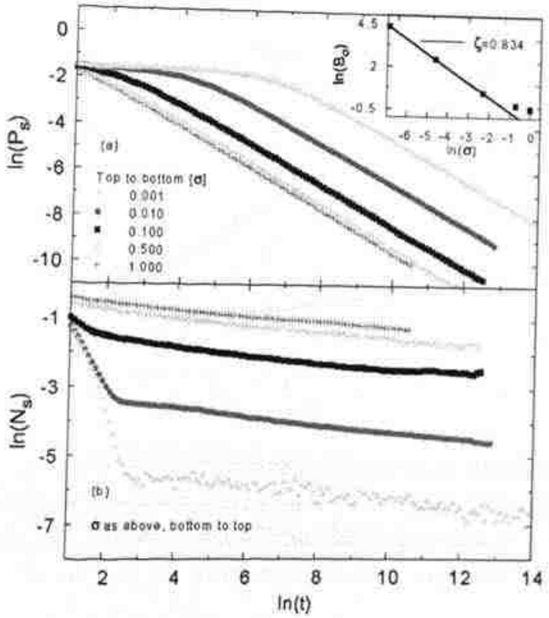

Figure 5.3. (Color online) Survival probability P_s and number of active sites N_s as functions of t for several points located on the generic phase boundary $\mu = 1.0000$ (2×10^6 to 10^7 runs used). Inset: prefactor B_σ vs. σ. The straight line is a fit to a power-law $B_\sigma \sim \sigma^{-\zeta}$.

$\rho(t) \sim 1/\ln(t/t_0)$ (with t_0 a microscopic time scale) expected for the GV universality class. This type of behavior is demonstrated in Fig. 5.5.

In summary, although all our results for the generic transition can be fitted both by pure power laws and by mean-field behavior with logarithmic corrections, the latter functional forms yield fits of somewhat higher quality. We also note that the critical exponents resulting from the pure power-law fits approximately fulfill the hyperscaling relation $\Theta - d/z = -\alpha - \delta$. However, the agreement is not very good (in particular, it is significantly worse than in one dimension [14]), indicating that the measured pure power-laws are not the true asymptotic behavior. Our results thus support the conjecture that the generic transition of the two-dimensional generalized contact process with two inactive states is in the GV universality class.

5.3.3. Transition at $\sigma = 0$. After addressing the generic transition, we now discuss in more detail the line of phase transitions occurring at $\sigma = 0$ and

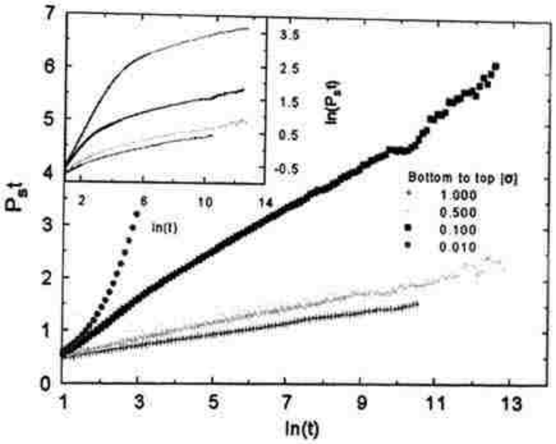

Figure 5.4. (Color online) Survival probability $P_s(t)$ for several points located on the generic phase boundary plotted as $P_s\, t$ vs. $\ln(t)$. Straight lines correspond to mean-field behavior with logarithmic corrections. Inset: Same data plotted as $\ln(P_s)\, t)$ vs. $\ln(t)$. Straight lines represent pure power laws.

$\mu_c^{cp} < \mu < \mu^*$. To study these transitions, we carried out several sets of simulations for fixed healing rate μ and several σ values approaching $\sigma = 0$.

We start by discussing the density decay runs. Figure 5.6 shows the stationary density ρ_{st} of active sites (reached at long times) as function of σ for several values of the healing rate μ. The figure shows that the stationary density depends linearly on σ for all healing rates in the interval $\mu_c^{cp} < \mu < \mu^*$, i.e., $\rho_{st} = B_\mu \sigma^\omega$ with $\omega = 1$ and B_μ being a μ-dependent constant. We also analyzed how the prefactor B_μ of this mean-field-like behavior depends on the distances from the simple contact process critical point and from the special point at $\mu = \mu^*$ and $\sigma = 0$. As inset (a) of Fig. 5.6 shows, B_μ diverges as $(\mu - \mu_c^{cp})^{-\kappa}$ with $\kappa = 1.56(5)$. According to inset (b), it vanishes as $(\mu^* - \mu)^{\kappa^*}$ with $\kappa^* \approx 0.23$ when approaching μ^*.

At the critical healing rate μ_c^{cp} of the simple contact process, the stationary density displays a weaker σ-dependence. A fit to a power-law $\rho_{st} \sim \sigma^{\omega_{cp}}$ gives an exponent value of $\omega_{cp} = 0.274(5)$.

Let us now compare these results with the behavior of spreading simulations in the same parameter region. Figure 5.7 shows the survival probability $P_s(t)$ and the number of active sites $N_s(t)$ for a fixed healing rate of $\mu = 0.8$ and several values of the boundary rate σ. After an initial decay, the number of active sites grows with time for all σ values, establishing that the system is in the active phase for

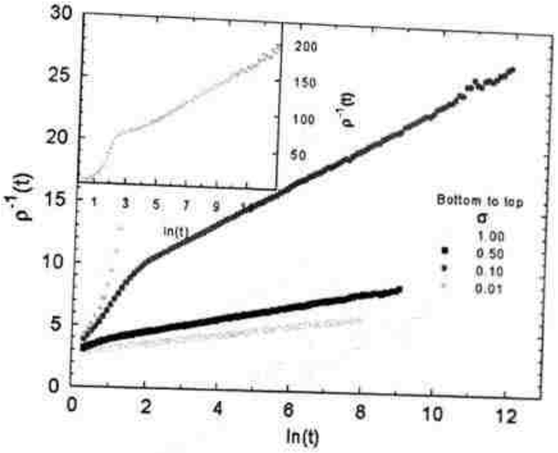

Figure 5.5. (Color online) Density of active sites plotted as $\rho^{-1}(t)$ vs. $\ln(t)$ for several points located on the generic phase boundary. The data are averages over 100 runs with system size 500 × 500. The curve for $\sigma = 0.01$ is shown in the inset because its density values are much smaller than those of the other curves.

all $\sigma > 0$. In agreement with this, the survival probability approaches a nonzero constant in the long-time limit. Remarkably, this stationary survival probability does *not* approach zero with vanishing σ. Instead, it approaches a σ-independent constant. We performed similar sets of simulations at other values of μ in the range $\mu_c^{cp} < \mu < \mu^*$, with analogous results.

We thus conclude that the behavior at the $\sigma = 0$ transition of the two-dimensional generalized contact process is very similar to the one-dimensional case. It can be understood in terms of the domain-wall motion as follows [14]. The relevant long-time degrees of freedom at $\mu > \mu_c^{cp}$ and $\sigma \ll 1$ are the domain walls between I_1 and I_2 domains. These walls can hop, branch and annihilate. The crucial observation is that the rates which control the domain wall dynamics are all proportional to σ for $\sigma \ll 1$, implying that their ratios are σ-independent. Consequently, the stationary state of the domain walls does not depend on σ for $\sigma \ll 1$. This explains why the survival probability P_s saturates at a nonzero, σ-independent value in Fig. 5.7. It also explains the σ-dependence of the stationary density ρ_{st} because active sites are created mostly at the domain walls at rate σ. Therefore, their stationary density is proportional to both σ and the stationary domain wall density ρ_{dw}, i.e., $\rho_{st} \sim \sigma \rho_{dw}$, in agreement with Fig. 5.6. Based on this argument, the exponent κ^* in inset (b)

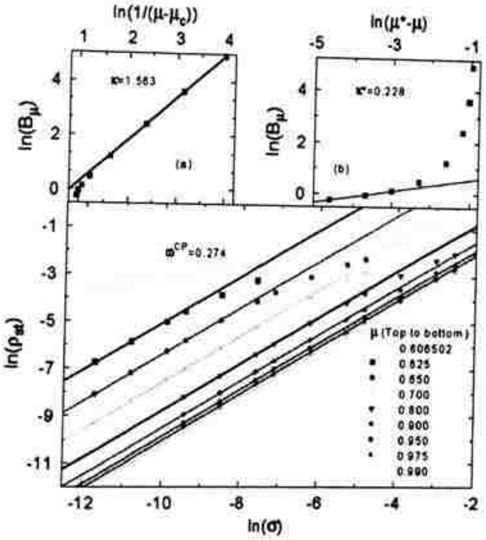

Figure 5.6. (Color online) Density decay simulations. Main panel: stationary density ρ_{st} as a function of the boundary rate σ for various healing rates μ. For $\mu_c^{cp} < \mu < \mu^*$, the solid lines are fits of the low-σ behavior to $\rho_{st} = B_\mu \sigma$. At the simple contact process critical point, $\mu = \mu_c^{cp} = 0.6066$, we fit to the power-law $\rho_{st} \sim \sigma^{\omega_{cp}}$ which gives an exponent of $\omega_{cp} = 0.274(5)$. The data are averages over 300 to 600 runs with system sizes 100×100. Inset a: prefactor B_μ of the linear σ dependence as a function of $\mu - \mu_c^{cp}$. A fit to a power law gives $B_\mu \sim (\mu - \mu_c^{cp})^{-\kappa}$ with $\kappa = 1.56(5)$. Inset b: prefactor B_μ as a function of $\mu^* - \mu$. A fit to a power law gives $B_\mu \sim (\mu^* - \mu)^{\kappa^*}$ with $\kappa^* \approx 0.23$.

of Fig. 5.6 should be identical to the exponent β of the generic transition line [14], which vanishes in mean-field theory. Our value, $\kappa^* \approx 0.23$ is thus somewhat too high which we attribute to it not representing the asymptotic behavior, in agreement with the significant curvature of the data in inset (b) of Fig. 5.6.

Just as in one dimension, the phase transition line at $\sigma = 0$ and $\mu_c^{cp} < \mu < \mu^*$ is thus not a true critical line. It only appears critical because the stationary density ρ_{st} (trivially) vanishes with σ. Correspondingly, the time evolution right on the transition line $\sigma = 0$ does not display critical power laws. also implies that the point $(\mu, \sigma) = (\mu^*, 0)$ is not a multicritical point, but a simple critical point in the same universality class as the generic transition.

5.3.4. Scaling of ρ_{st} at The Contact Process Critical Point $(\mu_c^{cp}, 0)$. The behavior of the stationary density of active sites ρ_{st} close to the simple contact process

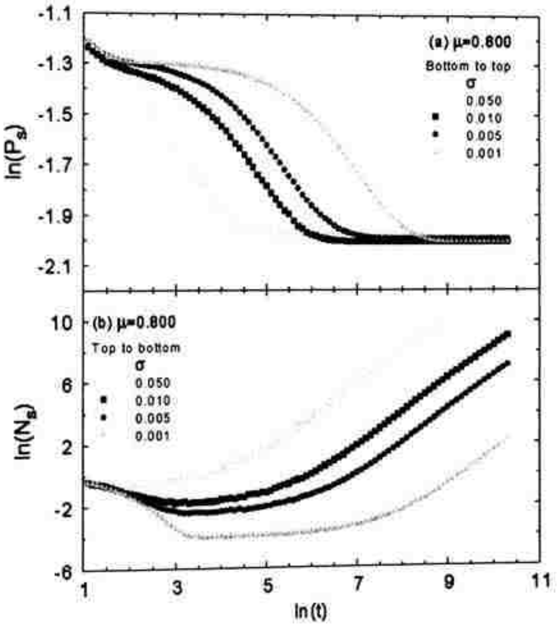

Figure 5.7. (Color online) Spreading simulations: Survival probability P_s and number of active sites N_s as functions of time t for a fixed healing rate of $\mu = 0.8$ and several σ. The data are averages over 2000 to 10000 runs on a 4000×4000 system.

critical point at $\mu = \mu_c^{cp}$ and $\sigma = 0$ can be understood in terms of a phenomenological scaling theory. We assume the homogeneity relation

$$\rho_{st}(\Delta\mu, \sigma) = b^{\beta_{cp}/\nu_{cp}^{\perp}} \rho_{st}(\Delta\mu\, b^{-1/\nu_{cp}^{\perp}}, \sigma b^{-y_{cp}}) \tag{157}$$

where $\Delta\mu = \mu - \mu_c^{cp}$, and b is an arbitrary scale factor. $\beta_{cp} = 0.584$ and $\nu_{cp}^{\perp} = 0.734$ are the usual order parameter and correlation length exponents of the two-dimensional contact process [22, 23], and y_{cp} denotes the scale dimension of σ at this critical point. Setting $b = \sigma^{1/y_{cp}}$ gives rise to the scaling form

$$\rho_{st}(\Delta\mu, \sigma) = \sigma^{\beta_{cp}/(\nu_{cp}^{\perp} y_{cp})} X\left(\Delta\mu\, \sigma^{-1/(\nu_{cp}^{\perp} y_{cp})}\right) \tag{158}$$

where X is a scaling function. At criticality, $\Delta\mu = 0$, this leads to $\rho_{st}(0, \sigma) \sim \sigma^{\beta_{cp}/(\nu_{cp}^{\perp} y_{cp})}$ (using $X(0) = \text{const}$). Thus, $\omega_{cp} = \beta_{cp}/(\nu_{cp}^{\perp} y_{cp})$. For $\sigma \to 0$ at nonzero

$\Delta\mu$, we need the large-argument limit of the scaling function X. On the active side of the critical point, $\Delta\mu < 0$, the scaling function behaves as $X(x) \sim |x|^{\beta_{cp}}$ to reproduce the correct critical behavior of the density, $\rho_{st} \sim |\mu - \mu_c^{cp}|^{\beta_{cp}}$.

On the inactive side of the critical point, i.e., for $\Delta\mu > 0$ and $\sigma \to 0$, we assume the scaling function to behave as $X(x) \sim x^{-\kappa}$. We thus obtain $\rho_{st} \sim (\Delta\mu)^{-\kappa}\sigma^{\omega}$ (just as observed in Fig. 5.6) with $\omega = (\beta_{cp} + \kappa)/(\nu_{cp}^{\perp} y_{cp})$. As a result of our scaling theory, the exponents ω, ω_{cp} and κ are not independent, they need to fulfill the relation $\omega_{cp}(\beta_{cp} + \kappa) = \beta_{cp}\omega$. Our numerical values, $\omega = 1$, $\omega_{cp} = 0.274$ and $\kappa = 1.56$ fulfill this relation in very good approximation, indicating that they represent asymptotic exponents and validating the homogeneity relation (157). The resulting value for the scale dimension y_{cp} of σ at the simple contact process critical point is $y_{cp} = 2.9(1)$.

5.4. CONCLUSIONS

To summarize, we investigated the two-dimensional generalized contact process with two inactive states by means of large-scale Monte-Carlo simulations. Its global phase diagram is very similar to that of the corresponding one-dimensional model. In particular, the generic ($\sigma > 0$) phase boundary between the active and inactive phases does not continuously connect to the critical point of the $\sigma = 0$ problem, i.e., the critical point $(\mu_c^{cp}, 0)$ of the simple contact process. Instead, it terminates at a separate end point $(\mu^*, 0)$ on the μ axis. As a result, the two-dimensional generalized contact process has two nonequilibrium phase transitions. In addition to the generic transition occurring for $\sigma > 0$, there is a line of transitions at $\sigma = 0$ and $\mu_c^{cp} < \mu < \mu^*$. We note that there is one interesting difference between the phase diagrams in one and two dimensions. In one dimension, the critical healing rate μ_c increases with increasing boundary rate σ. In contrast, the results of this paper show that the critical healing rate in two dimensions is completely independent of σ. The reason for this difference is presently an open question.

To determine the critical behavior of the generic transition, we performed simulations at and close to several points on the generic ($\sigma > 0$) phase boundary. We found the same critical behavior for all of these points, i.e, it is universal. Our data can be fitted reasonably well with pure power laws, giving the exponents $\Theta = -0.100(25)$, $\delta = 0.900(15)$, $\alpha = 0.080(4)$, and $z = 2.06(8)$. However, fits of equal and sometimes even better quality over longer ranges of time can be obtained by fitting to mean-field critical behavior, $\Theta = 0$, $\delta = 1$, $\alpha = 0$, and $z = 2$ with logarithmic corrections. We thus conclude that our results support the conjecture [17] that the critical behavior of the two-dimensional generalized contact process is in the generalized voter (GV)